Journal of Applied Physics

The transition from short- to long-timescale pre-pulses: Laser-pulse impact on tin microdroplets

Cite as: J. Appl. Phys. **131**, 105905 (2022); https://doi.org/10.1063/5.0082352
Submitted: 14 December 2021 • Accepted: 27 February 2022 • Published Online: 14 March 2022

Randy A. Meijer, Dmitry Kurilovich, Kjeld S. E. Eikema, et al.

Journal of Applied Physics ARTICLE scitation.org/journal/jap

The transition from short- to long-timescale pre-pulses: Laser-pulse impact on tin microdroplets

Cite as: J. Appl. Phys. **131**, 105905 (2022); doi: 10.1063/5.0082352
Submitted: 14 December 2021 · Accepted: 27 February 2022 ·
Published Online: 14 March 2022

Randy A. Meijer,[1,2,a)] Dmitry Kurilovich,[3] Kjeld S. E. Eikema,[1,2] Oscar O. Versolato,[1,2] and Stefan Witte[1,2,b)]

AFFILIATIONS

[1]Advanced Research Center for Nanolithography (ARCNL), Science Park 106, 1098 XG Amsterdam, The Netherlands
[2]LaserLab, Department of Physics and Astronomy, Vrije Universiteit, De Boelelaan 1105, 1081 HV Amsterdam, The Netherlands
[3]ASML Netherlands B.V., De Run 6501, 5504 DR Veldhoven, The Netherlands

Note: This paper is part of the Special Topic on Shock Behavior of Materials.

[a)]**Author to whom correspondence should be addressed:** r.meijer@arcnl.nl
[b)]**Electronic mail:** s.witte@arcnl.nl

ABSTRACT

We experimentally study the interaction of intense laser pulses with metallic microdroplets and the resulting deformation. Two main droplet deformation regimes have previously been established: that of sheet-type expansion after impact of "long" (typically >10 ns) pulses governed by incompressible flow and that of spherical expansion by internal cavitation after impact of "short" (typically <100 ps) pulses governed by shock waves, i.e., strongly compressible flow. In this work, we study the transition between these regimes by scanning pulse durations from 0.5 to 7.5 ns, where the boundaries of this range correspond to the limiting cases for the employed droplet diameter of 45 μm. We qualitatively describe the observed deformation types and find scaling laws for the propulsion, expansion, and spall-debris velocities as a function of pulse duration and energy. We identify the ratio of the pulse duration to the acoustic timescale of the droplet as the critical parameter determining the type of deformation. Additionally, we study the influence of fast rise times by comparing square- and Gaussian-shaped laser pulses. These findings extend our understanding of laser–droplet interaction and enlarge the spectrum of controllable target shapes that can be made available for future tin-droplet-based extreme ultraviolet sources.

I. INTRODUCTION

Laser-pulse impact has been widely employed to study the response of various materials to shock loading.[1–4] The high pressures attained for short durations commonly lead to cavitation and spallation events, which are studied in the context of phase transitions and material fracture. In nanolithography applications, the interaction of intense laser pulses with microdroplets,[5–16] shock loading them under certain conditions, is a subject of specific importance, with the goal of utilizing extreme ultraviolet (EUV) light with a wavelength of 13.5 nm. The light is typically generated in a multi-pulse scheme where an initial *pre-pulse* is used to deform a spherical tin microdroplet into a larger target more suitable for the following main laser pulse. This main-pulse turns the target into a hot plasma emitting the desired light at a wavelength of 13.5 nm with several percent conversion efficiency (CE) of converting "drive" laser light into usable EUV photons.[17] The optimization of the droplet deformation process entails the formation of an optimum target for the generation of EUV light and the minimization and mitigation of debris in the shape of high-energetic ions[13,18–20] and neutral tin (spray) droplets. Understanding the deformation process and its dependence on laser-pulse parameters is, therefore, of great value.

Several studies have been performed on the deformation after laser impact for "short" laser pulses in the femtosecond and picosecond regime[7–11,13,15,21,22] and for "long" pulses with several ns duration.[5,6,14,23,24] The studies reveal the existence of two main types of deformation: A shock-wave-induced cavity expansion

possibly accompanied by ejected spall, resulting in a double-dome-like structure in the case of "short" pulses, and deformation resulting from "long" pulses, where the droplet is deformed into a thin, extended sheet of only several tens of nanometers in thickness.[25] Aside from the identification of these two regimes, knowledge of the effects of pulse duration on laser-induced droplet deformation is limited.

In this work, we study the transition between the two deformation regimes by using laser pulses with durations ranging from 0.5 to 7.5 ns. The boundaries of this range correspond to the limiting cases described above for the employed droplet diameter of 45 μm. We qualitatively describe the wildly varying target shapes we observe in this short range of pulse durations. This range clearly captures the transition from shock-wave-dominated deformation types to sheet-like expansion. Furthermore, we compare deformation resulting from temporally Gaussian and square (constant intensity) shaped laser pulses. We quantify the deformation in terms of propulsion, expansion, and the velocity of ejected spall.

II. EXPERIMENTAL METHODS

Figure 1 shows a top-view schematic of the vacuum system and the laser beam path. A tin droplet with a diameter of 45 μm is hit by a laser pulse with a wavelength of 1064 nm from an in-house built laser system with temporal pulse shaping capabilities.[26] For this experiment, the laser system is operated at a repetition rate of 10 Hz. Gaussian-shaped pulses having durations τ_p of approximately 0.5, 1.3, 2, 3.5, 5, and 7.5 ns and "square," i.e., flat intensity, pulses having durations of approximately 2, 3.5, 5, and 7.5 ns full width at half maximum (FWHM) are used in this study. The square pulses have rise and fall times of approximately 200 ps. The pulse shapes are measured with a photodiode and an oscilloscope, and an exact width is obtained by fitting first- and higher-order Gaussian curves [see Figs. 1(b) and 1(c)]. The exact widths are used in the analysis, and the previously mentioned durations are used as labels throughout this work.

The energy of the laser beam is set by means of a waveplate-polarizer combination, after which the beam with a FWHM diameter of approximately 5 mm is focused down (f = 400 mm) in the center of the chamber to a Gaussian spot with a FWHM diameter of approximately 45 μm. A quarter waveplate before the lens is used to modify the polarization of the laser beam into circular, preserving cylindrical symmetry in absorption on the droplet surface. From a camera recording of the focal spot and a known droplet diameter, we find a geometric overlap factor of 0.44, which is used to determine the laser-pulse energy fraction impinging on the droplet E_{od}.

The droplet deformation is recorded using *shadowgraphy*, in which the droplet is back-lit perpendicular to the laser propagation axis and imaged with a long-distance microscope with a resolution of approximately 5 μm. The back-lighting light source emits 560 nm wavelength pulses with a duration of approximately 5 ns, setting the temporal resolution. By delaying the back-lighting source with respect to the focused laser beam, we record the deformation of the droplet after laser impact in a stroboscopic fashion, where each frame corresponds to a new laser–droplet interaction event. For more information on the experimental setup, we refer the reader to Ref. 27.

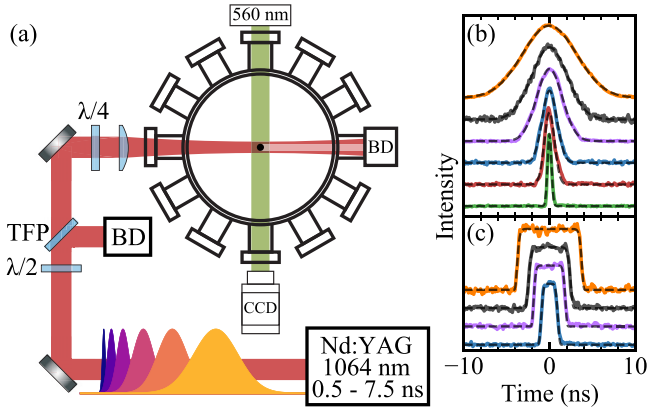

FIG. 1. (a) Top view of the vacuum chamber with the droplet (stream) in its center. The laser energy is set using a half-waveplate and thin film polarizer (TFP) combination. The beam is dumped in a beam dump (BD). (b) and (c) Measured Gaussian and square pulse shapes and fits of first and higher-order Gaussians. The intensity scale of each shape is normalized to the peak intensity and offset by a fixed amount.

III. TARGET MORPHOLOGY

A. Influence of pulse duration

Figure 2 shows the deformation of the liquid tin droplet following laser impact of Gaussian-shaped pulses with durations of 0.5 and 7.5 ns and an E_{od} of 1.3 mJ. The two displayed deformation processes are clearly distinct. Impact of a 0.5 ns pulse results in a spherical, bubble-like expansion attributed to cavity formation in the center of the droplet.[7–11,13] The laser impact excites a shock wave on the laser-facing surface, which then propagates through the droplet. Due to the spherical shape of the droplet, the shock wave and the

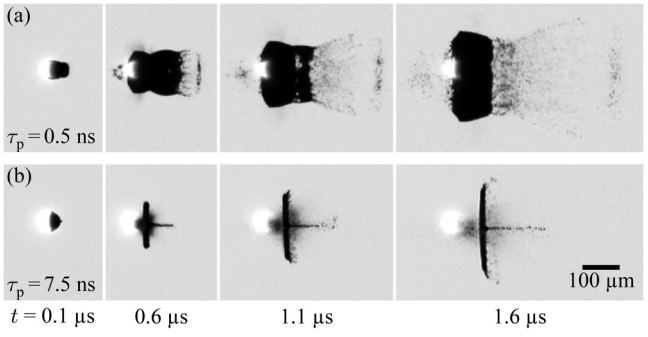

FIG. 2. Deformation following laser impact of temporally Gaussian-shaped pulses with FWHM durations of (a) 0.5 ns and (b) 7.5 ns and an E_{od} of 1.3 mJ. Laser is incident from the left. The bright overexposed spot is light emitted from the plasma cloud. Due to the relatively long exposure time of the camera (≈ms), the light is visible in all frames, although present only for a duration similar in length to the laser pulse itself.

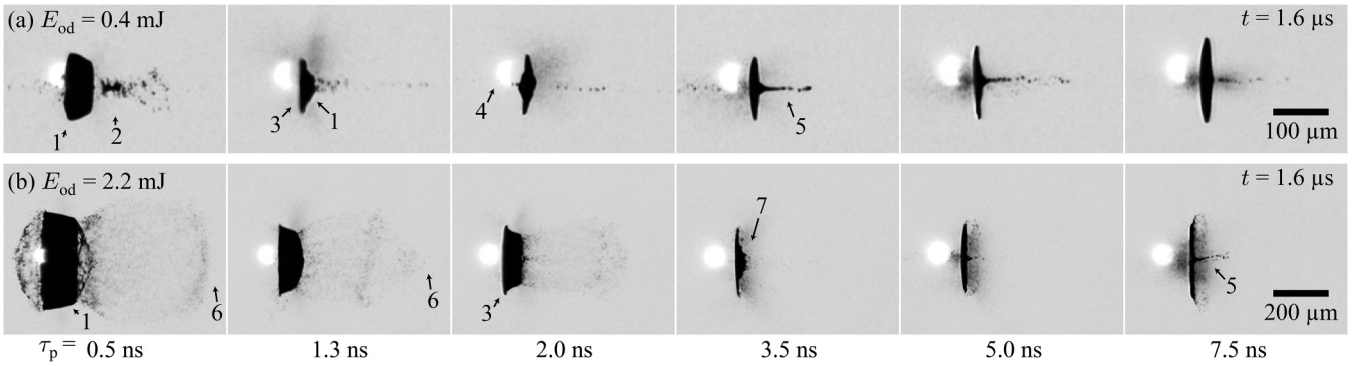

FIG. 3. Shadowgrams of droplet deformation 1.6 μs after laser impact for the studied pulse durations and E_{od} values of (a) 0.4 and (b) 2.2 mJ. Scale in (b) is twice that of (a). Laser is incident from the left. The pulse duration is indicated below each column. Several features are explicitly indicated in selected images by the following numbers: (1) central cavity, (2) collapsed spall, (3) edge flattening, (4) plasma emission, (5) jet, (6) spall front, and (7) central cavity remains.

accompanying rarefaction wave focus in the center of the droplet, resulting in internal cavitation. The shock wave subsequently reflects off the back side of the droplet, and a spall layer is ejected.[7–9,11]

The impact of a 7.5 ns pulse primarily leads to propulsion and cylindrical expansion into a thin sheet, a relatively well understood process.[5,6,14,23,24] The formation of a jet is also clearly visible and was observed before in similar experiments.[13,14,28] Jet formation is commonly observed following cavity collapse.[29–32] This, along with the accompanying spray, is a possible indication that a cavity is also formed in this case, albeit smaller and expanding at a slower rate before collapsing.

Figure 3 illustrates the transition of deformation resulting from impact of temporally Gaussian-shaped pulses when increasing the pulse duration from 0.5 to 7.5 ns. Two cases corresponding to E_{od} values of 0.4 and 2.2 mJ are shown. A general trend from shock-wave-dominated deformation, exhibiting cavitation and spallation to flattening and propulsion, is present with increasing pulse duration. During this transition, we clearly observe the co-existence of both types of deformation.

The deformation after impact of a 0.5 ns pulse again exhibits strong spherical expansion due to shock-wave-induced cavitation in the interior of the droplet. Furthermore, a layer of liquid is spalled off and rapidly fragments as it expands. In Fig. 3(a), the remains of this spall are located on the laser axis due to its partial collapse, while in Fig. 3(b), the spall is visible as a cloud of fragments. A jet is also present in some cases, possibly originating from the collapse of a central cavity or spall layer as mentioned previously. In Fig. 3 (b), a shrinking of the spall cloud, indicating a decrease in its velocity, is clearly visible with increasing pulse duration and the spall is absent for longer pulse duration. Moreover, with increasing pulse duration, flattening of the laser-facing surface becomes more apparent and spherical expansion decreases until eventually, the observed shape becomes that of a flat sheet.

B. High-energy deformation features

Additional deformation effects appear when the incident energy is increased significantly. Figure 4 shows deformation for significantly higher values of E_{od}. Overall comparable trends are visible, with flattening of the resulting shape with increasing pulse duration. A previously unobserved cloud, rapidly expanding radially and against the laser propagation direction, is now clearly present for the 0.5 ns pulse case. The exact origin of this cloud, which is absent for lower energies, is unknown. We speculate that a partial reflection of the rarefaction wave from the already forming cavity plays a role in the formation of this cloud, which becomes less pronounced when the incident pulse duration increases.

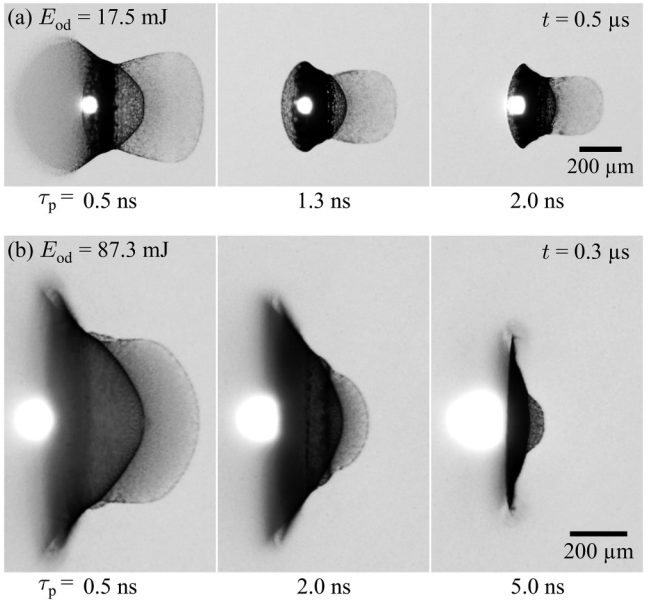

FIG. 4. Side-view shapes following impact of temporally Gaussian-shaped pulses with various pulse durations and energies. Images are recorded at t = 0.5 and t = 0.3 μs after laser impact for (a) and (b), respectively. The pulse duration τ_p is indicated below each image.

In the highest energy cases studied [Fig. 4(b)], strong fragmentation of the droplet is observed. Although spherical expansion due to cavitation seems to still be present (the resulting curvature and the on-axis expansion of the target are still observable), no fragments moving against the laser propagation direction are visible as opposed to the lower-energy cases [Figs. 3(b) and 4(a) 0.5 ns]. Significant amounts of hot and dense plasma are generated at these high energies, as also evidenced by the brighter and expanded plasma glow visible in the shadowgrams, which likely plays a role in the absence of these fragments.

C. Gaussian vs square pulses

A significant difference in deformation following impact of temporally Gaussian- or square-shaped pulses is observed and highlighted in Fig. 5. From the comparisons presented in Figs. 5(a)–5(c), it becomes clear that, for equal FWHM pulse widths, the deformation after impact of a square pulse displays a larger spall, faster spall front, and stronger spherical expansion when compared to the Gaussian case. Accordingly, deformation in the Gaussian case displays more flattening of the laser-facing side when compared to the square case. This last point is most clearly demonstrated by the cases presented in panels (b) and (c). Together, the trends described above indicate that the fast rise time and overall faster energy deposition of the square pulses lead to higher peak pressures of the shock wave(s) propagating in the droplet.

In Fig. 5(d), we show that impact of a square-shaped laser pulse with a duration of 7.5 ns leads to spall formation, which is absent in the Gaussian case. This hints at the formation of a sharply peaked pressure wave, which is necessary for spallation to occur when it reflects on the rear side of the droplet. This conclusion is discussed further in Sec. VI

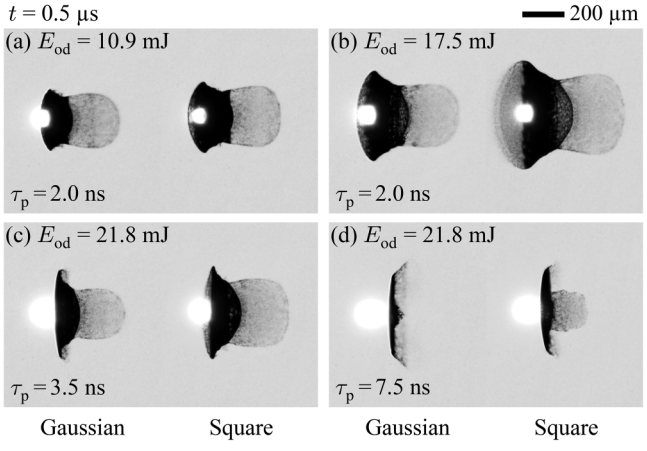

FIG. 5. (a)–(d) Shadowgrams comparing deformation using Gaussian and square temporal pulse shapes for various combinations of FWHM pulse duration τ_p and E_{od}. All images are recorded at $t = 0.5\,\mu s$ after laser impact and are displayed at equal scale. Note that the target for the square case in (d) is slightly tilted around the vertical direction due to a slight laser-to-droplet misalignment.

IV. LASER-DRIVEN TARGET PROPULSION

The deformation of the droplet following laser impact is typically accompanied by a propulsion, or induced center-of-mass velocity, of the tin mass along the laser propagation axis. This propulsion U has been studied in detail for the case of a Gaussian-shaped pulse with a FWHM duration of 10 ns.[6,24] In these studies, the laser-energy dependence of the on-axis propulsion was found to be accurately described by a power-law scaling with an exponent of 0.60(1).[24] Furthermore, it was found that the energy impinging on the droplet E_{od} can be used instead of the total laser-pulse energy to account for varying focal spot sizes, leading to the expression

$$U = K_U E_{od}^{0.6}. \quad (1)$$

Additionally, in Refs. 6 and 24, an offset pulse energy $E_{od,0}$ was introduced to accurately describe the sudden loss of propulsion at low energies close to the ablation threshold. Since in this work, we do not probe this threshold regime, we omit this parameter for simplicity.

To obtain the propulsion U for the pulse durations studied in this work, we apply an analogous analysis of the shadowgrams as in Refs. 6 and 24. Appropriate thresholds are applied to the shadowgrams to isolate the shadow from the background illumination, and the center of mass (first moment) of the thresholded image is determined as a function of shadowgraphy delay time. The resulting displacement data follow a straight, ballistic trajectory, which is fit by a linear function to obtain U (also see Ref. 24).

Figure 6(a) shows U as a function of laser intensity E_{od}/τ_p for the various pulse durations and both Gaussian and square temporal pulse shapes. The choice to plot U as a function of pulse intensity instead of energy is made first because a deviation from the established trend is observed for high intensities [more clearly visible in Fig. 6(b) and discussed later], and second, because it separates the propulsion curves benefiting graphic clarity. We find that U increases with pulse duration and that U resulting from Gaussian and square pulses is comparable for equal E_{od}/τ_p. This indicates that the FWHM duration is an appropriate pulse-width measure when comparing U between Gaussian and square pulses in this duration regime. Note that with a FWHM definition of τ_p, the Gaussian pulses have a similar (94%) peak intensity as square pulses at equal pulse energy.

Following the choice of the x axis, we rewrite Eq. (1) into

$$U = K_{U,I}\left(\frac{E_{od}}{\tau_p}\right)^{0.6}, \quad (2)$$

from which follows $K_U = K_{U,I}\tau_p^{-0.6}$. We fit Eq. (2) to the data in Fig. 6(a) and find a good agreement for all pulse durations up to intensity values of 20 mJ ns^{-1}. Values above this range seem to deviate; therefore, with an additional margin, we exclude values above 10 mJ ns^{-1} from the final fitting procedure of which the results are shown in Fig. 6(a). Note that in the propulsion studies reported in Refs. 6 and 24, the maximum laser intensity studied is below the current regime where a deviation is observed; i.e., $E_{od}/\tau_p < 10$ mJ ns^{-1}.

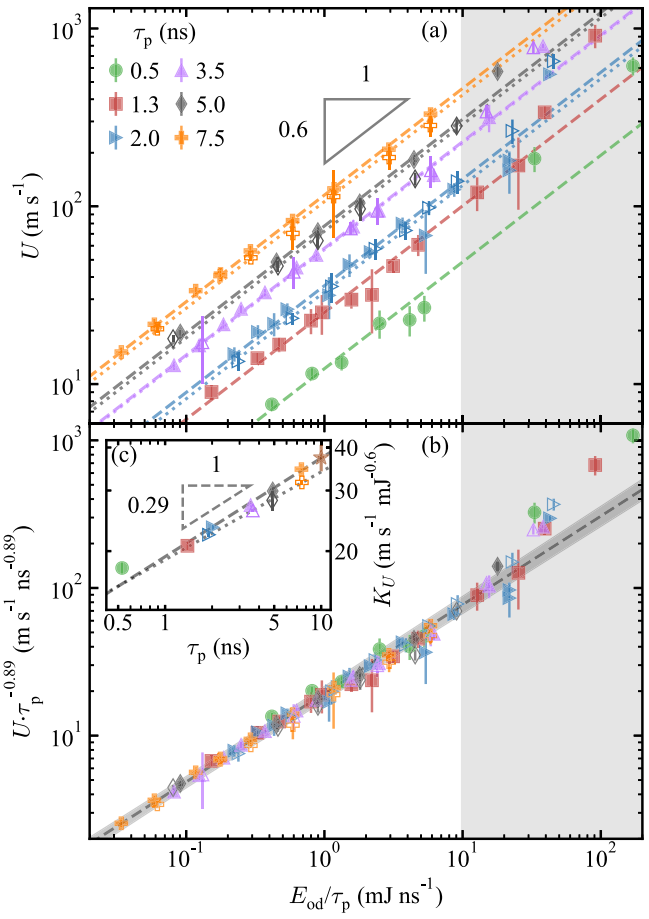

FIG. 6. (a) Center-of-mass propulsion velocity U as a function of E_{od}/τ_p for the Gaussian (filled markers) and square (open markers) pulse shapes. The vertical error bars indicate the fit parameter standard error from the linear fit to the center-of-mass displacement curve. For each combination of pulse duration and shape (Gaussian or square), the data are independently fit with Eq. (2). Data points in the gray region are excluded from these fits (see the main text). The fit results are plot using a dashed or dotted line for the Gaussian and square pulse shapes, respectively. (b) Similar to (a) with scaled velocities $U\tau_p^{-0.89}$. (c) Proportionality constants K_U obtained from fits in (a) as a function of τ_p and fits of Eq. (3) for the Gaussian- and square-shaped pulses independently indicated by the dashed and dotted lines, respectively. The result for a 10 ns Gaussian-shaped pulse obtained in Ref. 24 is indicated in (b) and (c) by the dashed line (with the corresponding shaded region indicating the error) and the star-shaped data point, respectively. In (c), the star-shaped data point is not included in the fit of Eq. (3).

The proportionality constants K_U obtained from the fits are plotted as a function of pulse duration in Fig. 6(c). As a power-law scaling of K_U with τ_p is apparent, we write

$$K_U = L_U \tau_p^{\beta}. \tag{3}$$

Fits of Eq. (3) to the data for Gaussian and square pulse shapes independently provide values for β and L_U. The results are shown in Table I. We find no significant difference regarding L_U and β for the two different pulse shapes, again indicating that impact of Gaussian- or square-shaped pulses results in (close to) equal propulsion velocities when the FWHM definition is used for τ_p.

The obtained value(s) of β can be used to collapse all data onto a single curve using the appropriate scaling of $U\tau_p^{0.6+\beta}$. Here, we use the result $\beta = 0.29$ obtained for Gaussian pulse shapes, which results in an excellent collapse of all data points as shown in Fig. 6(b). After collapsing all data, the previously mentioned deviation at high intensities is clearly visible. For $E_{od}/\tau_p \gtrapprox 20$ mJ ns^{-1}, U increases at an approximately linear rate, faster than the established power of 0.6. The increased scaling possibly originates from a significant increase in the ablated mass fraction in this regime and could, in future work, be investigated with dedicated simulations.[24,33] It is also possible that a systematic overestimation of U arises during the shadowgraphy analysis due to the extreme deformation and fragmentation as shown in Fig. 4. In Figs. 6(b) and 6(c), we additionally plot the result for a 10 ns pulse duration from Ref. 24 and find an excellent agreement with the current dataset. Since in Ref. 24, the majority of the data was obtained using a droplet diameter of 47 μm, a correction of K_U is applied to enable comparison with the droplet diameter of 45 μm used in this work. For this correction, we apply a scaling of $K_U \propto R_0^{-2.2}$ with droplet radius R_0, as predicted in Ref. 24 and experimentally confirmed in Ref. 25.

In Ref. 24, a scaling of $K_U \propto \tau_p^{\beta}$, with $\beta = 1 - 0.6 = 0.4$, was predicted, where the value of 0.6 follows from the exponent in Eq. (1). The values of β obtained here are close, but not in full agreement with this prediction, which was made assuming that the exponent of 0.6 does not vary with τ_p. Although we find a good agreement with our measurements when applying this assumption, we cannot yet exclude minor deviations of the exponent in Eq. (1) for which a more extensive and more accurate dataset is needed. The discrepancy between the prediction and our measurement is possibly inherent to the pulse-duration regime studied here. It has been shown[33] that a quasi-stationary ablation front forms when the pulse duration τ_p is significantly longer than the hydrodynamic timescale of the plasma τ_h, i.e., $\tau_p \gg \tau_h$, where τ_h follows from the typical flow length scale and the flow velocity of the laser-produced plasma, and typically ranges from 0.1 to 1 ns. This means that the assumption $\tau_p \gg \tau_h$ made in the prediction of Ref. 24 does not hold for the full range of pulse durations and energies studied here, leading to a deviation from the predicted scaling. It is, therefore, possible that a determination of β for longer pulses will result in a different value. Altogether, the extension of the behavior of U from previous studies[6,24] to the pulse-duration regime studied here is remarkable considering the wildly varying deformation types.

TABLE I. Results of fits of Eq. (3) to the data shown in Fig. 6(c). The given errors are the standard error of the fit parameter.

	β	L_U (m s^{-1} mJ$^{-0.6}$ ns$^{-\beta}$)
Gaussian	0.29(2)	19.3(5)
Square	0.26(1)	18.9(7)

V. TARGET EXPANSION DYNAMICS

The expansion of liquid droplets following laser impact has previously been studied for both of the "asymptotic" cases of the present work, that of expansion into a thin sheet[5,6,14,23,24] and that of spherical bubble-like expansion due to cavitation.[9] In both cases, the observed late-time expansion trajectories can be well described using analytic fluid-mechanical models. In the pulse-duration transition regime measured here, the observed shapes strongly depart from these two specific cases (of a stretching sheet and a bubble) and display strong non-trivial variations. As such, no analogous fluid-mechanical model would warrant a comparison with the current measured expansion trajectories. Furthermore, in the aforementioned fluid-mechanical models, the initial rate of radial expansion immediately after laser impact $\dot{R}(t=0)$, hereafter referred to as $\dot{R}_0$, was shown to be the most relevant observable, which sets the expansion trajectory until significant fragmentation occurs. Naturally, when the expansion rate is large enough, fragmentation occurs before any significant deceleration of the expanding liquid takes place, and the complete expansion trajectory becomes ballistic with a velocity $\dot{R}_0$. Motivated by the above, we limit ourselves to an analysis of $\dot{R}_0$, which is obtained by a linear fit to an early time range of the expansion curve, before any significant deceleration of the expanding liquid takes place due to the effects of surface tension acting on a capillary timescale $\sim 10\,\mu$s.[6,9]

Due to the strongly varying shapes, it is difficult to set a clear universal size measure. In general, the size of the target is determined at its widest point, excluding fragments detached from ligaments that sometimes form on the edge of the sheet-like targets and excluding the spall when present. For shapes exhibiting a spherical-like expansion that display a clear size difference between the widest overall point and the widest point of the expanding central cavity, the relevant width is taken to be that of the central cavity. This is, for example, the case in Fig. 4(a) at $\tau_p = 0.5$ ns, where the widest point of the central cavity approximately corresponds to the "waist" of the total observed shape.

Figures 7(a) and 7(b) show $\dot{R}_0$ as a function of E_{od} for the Gaussian- and square-shaped pulses, respectively. It is clear that, analogous to U, $\dot{R}_0$ follows a power-law dependence with laser energy. We, therefore, write

$$\dot{R}_0 = K_{\dot{R}} E_{od}{}^{\gamma}. \tag{4}$$

Although some variation between the different pulse durations is especially apparent for the Gaussian-shaped pulses, all data can be reasonably described by a single power-law curve. This correspondence to a single power law is remarkable, given the very different overall target shapes observed for different pulse durations. A single fit of Eq. (4) to all data points in Figs. 7(a) and 7(b) combined results in $\gamma = 0.70(1)$ and $K_{\dot{R}} = 42(2)\,\mathrm{m\,s^{-1}\,mJ^{-\gamma}}$ and is indicated by the black dashed line.

To investigate any changes with pulse duration and pulse shape, fits of Eq. (4) to each separate pulse duration and shape are also performed. The results are shown in Figs. 7(c)–7(h). Unsurprisingly, almost all values of γ are very similar, and a more accurate determination is needed to confirm any overall trend with τ_p and pulse shape. However, for the Gaussian and square 7.5 ns pulses, we find significant below-average values for γ of 0.65(1) and 0.64(2), respectively, whereas all other cases are consistent with $\gamma \geq 0.7$. Likewise, a clear trend in $K_{\dot{R}}$ is absent, although the values for the shortest and longest pulses (0.5 and 7.5 ns) show moderately larger values, indicating that radial expansion in the transition regime is possibly less efficient.

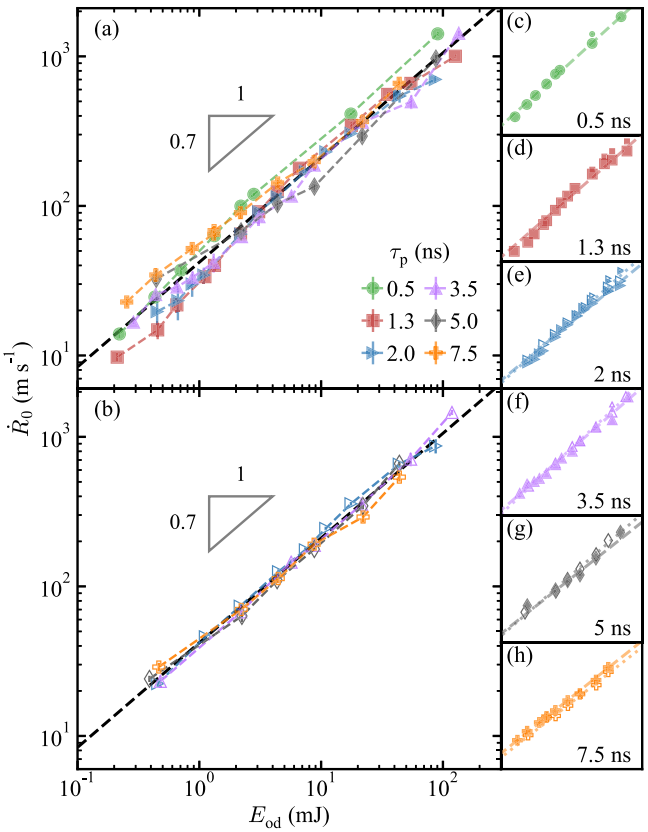

FIG. 7. Initial expansion velocity $\dot{R}_0$ as a function of E_{od} for all pulse durations and (a) Gaussian (filled markers) and (b) square (open markers) pulse shapes. (c)–(h) Individual plots of each pulse duration. Scale in (c)–(h) is equal to (a) and (b).

For the short-pulse regime, the physical origin of the scaling parameter γ is likely complex due to its sensitivity to the equation of state of the liquid, the specific spherical geometry, and the details of the laser-ablation process. Previous studies have also reported on values for γ in the short-pulse regime and under similar experimental conditions. In one case,[9] a value of 0.46(2) was reported for 15 ps pulses, and another study[15] reported on values ranging from 0.74(4) to 0.63(2) for pulse durations ranging from 220 fs to 10 ps. Although the step in pulse duration between these studies and the current study is large, from ≤ 15 ps to 0.5 ns, the similarity in the observed deformation warrants a comparison. We find $\gamma = 0.74(2)$ for $\tau_p = 0.5$ ns in reasonable agreement with Ref. 15, but less so with Ref. 9. This further stresses the possible complexity of γ and calls for additional experiments to clarify this

disparity between the reported values. For a more detailed comparison of initial expansion velocities between 220 fs and 0.5 ns pulses, see Ref. 34.

For the long-pulse regime, the physical origin of γ is likewise complex. However, from the analogy with studies on the impact of water droplets on rigid pillars,[35] we expect that $\dot{R}_0 \simeq U$ as follows from energy conservation arguments. Therefore, following Sec. IV and by equating Eq. (1) with Eq. (4), we predict that for the case of sheet-like expansion, $\gamma \approx 0.6$. The decrease of γ from ≥ 0.7 down to approximately 0.65 that we observe for the $\tau_p = 7.5$ ns pulses is in agreement with this expectation.

A. Expansion vs propulsion

Previous work[5,36] has shown that, dissimilar to the pillar-impact case,[35] the ratio $\dot{R}_0/U$ for the laser-impact case of sheet expansion is influenced by the size ratio of the focal spot and droplet. A smaller laser focal spot leads to an increasingly focused pressure field, which subsequently results in a larger $\dot{R}_0/U$ ratio. Furthermore, a scaling of the ratio $\dot{R}_0/U$ to laser-pulse energy has been shown to exist.[14] This is due to the expansion dynamics of the plasma formed during the laser–droplet interaction process. During laser impact, a plasma cloud is formed that expands around the droplet and exerts the relevant pressure on the droplet surface. As a result of this plasma expansion, the spatial pressure profile imparted on the droplet is broadened and can, in fact, extend beyond the laser-facing side.[24] The extent to which the initial droplet-to-focal-spot size ratio influences $\dot{R}_0$ in the shock-wave-dominated regime is unclear but likely dissimilar to its effect for longer pulses. Furthermore, it is straightforward to conclude that the above-mentioned plasma-expansion effects are absent when $\tau_p \lesssim \tau_h$. Accordingly, we cannot ignore these effects when comparing the expansion velocity between different pulse durations. For the 7.5 ns Gaussian pulse, which induces sheet-like deformation most comparable to that studied in Ref. 14, we observe $\dot{R}_0/U = 1.4(2)$ with no significant dependence on laser energy. The absence of such a dependence, in contrast to Ref. 14, could be the result of the combination of the relatively tight focusing condition, the droplet size, and the pulse duration used here. These conditions limit the growth of the plasma cloud during the pulse to which the laser-energy dependence observed in Ref. 14 was attributed. The absence of an $\dot{R}_0/U$ dependence on laser energy in our case contributes to the agreement $\gamma \approx 0.6$ we have observed for the 7.5 ns pulses.

In summary, changing the focusing conditions to a more tightly focused beam, or increasing the droplet size, might increase $\dot{R}_0/U$ such that long pulses will induce a faster expansion compared to short pulses at equal energy. Complementarily, a more loosely focused laser beam, or a smaller droplet, will only reduce expansion for long pulses, whereas expansion for short pulses is probably largely unaffected.

VI. SPALLATION DYNAMICS

Tracking of the on-axis position of the spalled material, already previously referred to as the spall front and indicated in Fig. 3(b), was performed to obtain a spall velocity. The spall-front velocity u_s is (analogous to our determination of $\dot{R}_0$) obtained by a linear fit to an early time range of the spall-front trajectories and shown in Fig. 8. As expected and shown in Figs. 8(a) and 8(b), u_s increases with E_{od}. Moreover, a decrease with increasing τ_p is observed, and for the 7.5 ns Gaussian pulse, no spallation was observed. Since the velocity of the spall will depend on the peak pressure of the shock wave[37] and the ablation pressure that excites the shock wave is assumed to depend on the laser intensity,[24,33] we expect a laser intensity-dependent trend for u_s. Indeed, a clear collapse is observed for u_s as a function of pulse intensity as shown in Figs. 8(c) and 8(d). However, a significant deviation of the curves for the 0.5 and 5 ns Gaussian pulses from the other collapsed curves is present. These deviations—and at the same time the remarkable overlap of all square pulses—suggest that a characteristic timescale τ_{ch} exists that dictates effective coupling of the laser pulse to the shock wave causing the spall. An upper limit for τ_{ch} is then set by the shortest square pulse, and a lower bound is set by the shortest, deviating Gaussian pulse, meaning $0.5\,\text{ns} < \tau_{ch} < 2\,\text{ns}$.

The continued presence of spallation for longer square pulses indicates the formation of a sharp-peaked shock wave following a fast rise time, even under the condition of continued loading by ablation pressure. In a one-dimensional geometry, hydrodynamic attenuation combined with a significant propagation distance allows for a conversion of an initial uniform shock wave into a peaked, triangular-shaped shock wave.[38,39] However, this process takes place on a timescale significantly longer than the duration of the applied pressure pulse and therefore, since for the longest pulse durations applied here $\tau_p \sim \tau_a$, with $\tau_a = R_0/c \approx 9$ ns, the acoustic timescale at which pressure waves traverse the droplet does not explain the formation of a peaked pressure pulse in our case. In Ref. 21, where a model for impact of continuous pressure pulses on droplets is developed, a separation of a leading narrow pressure peak with a width on the order of $0.1R_0$ is observed during the laser pulse. Since in this case, the details of the laser-ablation process are not modeled, but a temporally constant pressure is applied; it indicates that pure hydrodynamics and the spherical geometry play a deciding role in the formation of a leading shock wave under continuous loading. Accordingly, the shape and evolution of this shock follow a hydrodynamic similarity analogous to that presented in Ref. 11. As the leading shock is considered responsible for the generation of the spall, the aforementioned characteristic timescale τ_{ch} should be directly related to the width of the shock wave and scale with the droplet radius R_0. In Ref. 11, where impact of femtosecond-duration pulses ($\tau_p \ll \tau_a$) on tin microdroplets is simulated using smoothed-particle hydrodynamics, the resulting triangular-shaped pressure wave attains a width on the order of $0.1R_0$, similar to that in Ref. 21. We, therefore, expect $\tau_{ch} \sim 0.1R_0/c_s$ with c_s being the propagation velocity of the shock wave. With the present droplet diameter of 45 μm and approximating c_s by the speed of sound ($2500\,\text{m}\,\text{s}^{-1}$), we obtain $\tau_{ch} \sim 1$ ns. This is in agreement with the aforementioned upper and lower boundaries observed from the experiment. As c_s increases with peak pressure, some variation in τ_{ch} is expected as a function of laser intensity. Additionally, a significant variation of τ_{ch} is expected to arise when the laser focal spot becomes significantly smaller than the droplet size, giving rise to an

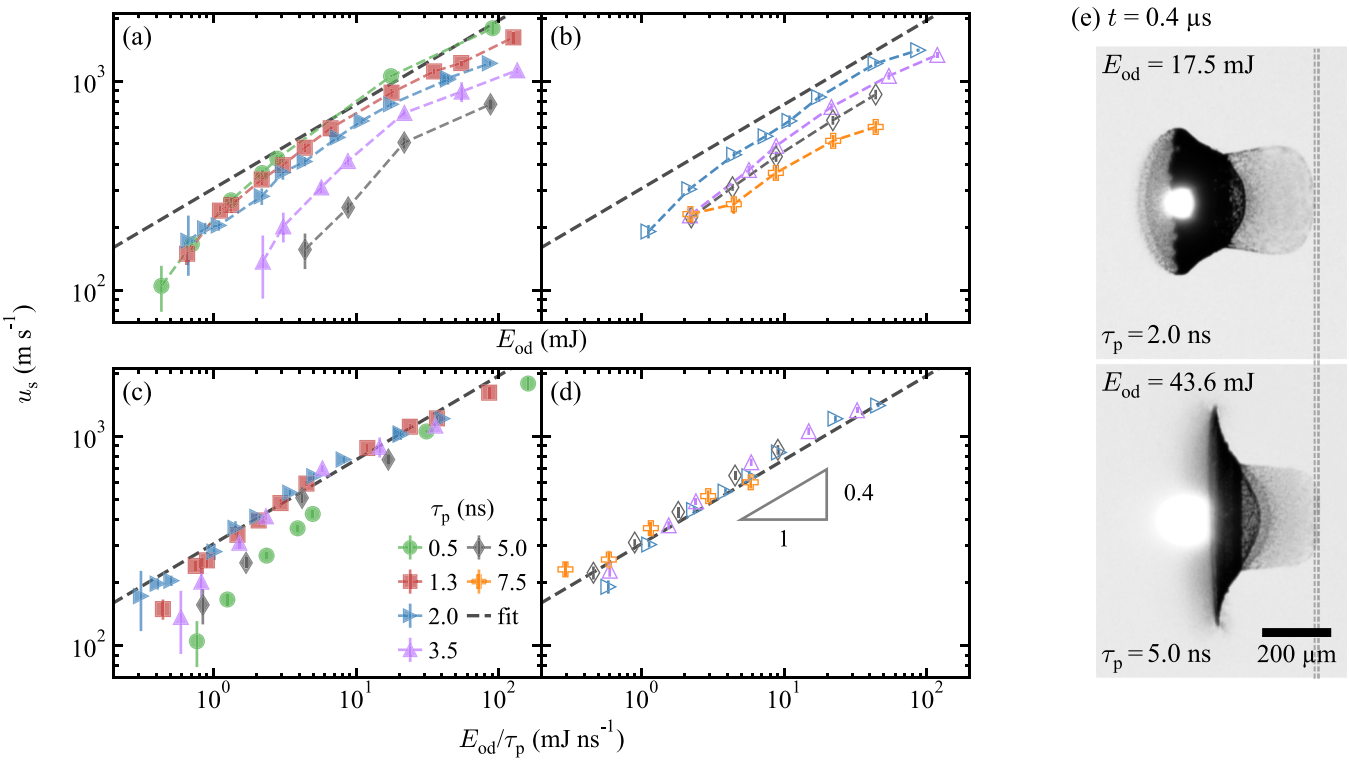

FIG. 8. Spall-front velocity u_s as a function of E_{od} for (a) Gaussian and (b) square pulse shapes. u_s as a function of E_{od}/τ_p is shown in (c) and (d) for the Gaussian and square shapes, respectively. Note that data for the 7.5 ns Gaussian pulse are absent from the plot since there was no spall observed for this pulse. The gray dashed line indicates the fit of Eq. (5) to the data in (c) and (d) with exclusion of the 0.5 and 5 ns Gaussian pulses (see the main text for details). For reference, the fit result is also plot in (a) and (b) taking $\tau_p = 1$ ns. (e) Shadowgrams of two different pulse parameters with equal laser intensity, demonstrating the matching spall velocity.

increasingly "narrow" ablation pressure profile along the droplet surface. Evidently, this results in non-trivial changes of the internal pressure evolution.

For the spallation dynamics, again, a power-law dependency is observed as a function of laser energy and intensity. Motivated by the demonstrated collapse, we limit ourselves to an analysis considering laser intensity only and write

$$u_s = K_s \left(\frac{E_{od}}{\tau_p}\right)^{\eta}. \tag{5}$$

A fit to the data of Figs. 8(c) and 8(d) combined, excluding the most deviating curves of the 0.5 and 5 ns Gaussian pulses, gives $\eta = 0.40(1)$ and $K_s = 306(7)$ in units of m s^{-1} ns$^{\eta}$ mJ$^{-\eta}$. Interpretation and clarification of the obtained fit parameters, through detailed simulation work, is out of the scope of the current work.

VII. DISCUSSION AND CONCLUSIONS

From the range of observations on the pulse-duration dependence of target propulsion, expansion, and spallation, we find that the studied range of pulse durations between 0.5 and 7.5 ns truly forms the transition regime between the observed sheet-like expansion[6,14,23] and the cavitation-driven bubble-like expansion[7–9,11] for the employed droplet diameter of 45 μm. The main reason for this transition appears to be the ratio of the pulse duration τ_p to the liquid acoustic timescale at which pressure waves propagate through the droplet $\tau_a = R_0/c$, setting the droplet size dependence of the transition regime. For the studied droplet diameter of 45 μm, τ_a is approximately 9 ns. When a regime of shock waves is entered, we should, however, consider a shock velocity $c_s > c$, which will result in an effective decrease of τ_a. Furthermore, c_s exhibits a pressure dependence and, therefore, a laser-intensity dependence, shifting the transition to shorter times for higher laser-intensities. Lastly, the threshold of cavitation has a strain rate dependence,[11,40] which can, to some extent, effectively shift the transition as well.

Evidently, no hard separation between the regimes exists. Sheet-type expansion, which has previously been explained by assuming incompressibility and considering only the time-averaged pressure fields, follows when $\tau_p \gtrsim \tau_a$. Yet, when $\tau_p \sim \tau_a$, minor indirect signs of cavitation remain in the form of spray and jetting. When $\tau_p \lesssim \tau_a$, compressible flow becomes significant, and the time-dynamics of the internal pressure profiles, i.e., shock waves, will increasingly dominate the deformation by inducing cavitation

and spallation. Effects of laser-to-droplet alignment[41,42] are not expected to have any significant effect on the transition itself but may influence details of the target morphology.

Furthermore, we have extended the knowledge on laser-driven-propulsion to the explored pulse duration regime and find a reasonable agreement to previously determined scalings of propulsion with laser energy and pulse duration. We find that propulsion resulting from impact of square- and Gaussian-shaped pulses is comparable when taking the full-width-at-half-maximum pulse-width definition at which a similar peak intensity is reached at equal pulse energy.

The radial expansion velocities were found to show a remarkable insensitivity to the pulse duration and shape and depend almost solely on the laser-pulse energy. The scaling of the expansion velocity with the laser-pulse energy was found to be in agreement with expectations and in reasonable agreement with previously obtained results, although we stress that these observations cannot be considered independent of the droplet size and the droplet-to-focal-spot size ratio.

Lastly, we have also shown that when using fast-rise-time square pulses with a sufficient intensity, spall is always formed, even for longer pulses when $\tau_p \sim \tau_a$ and the main expansion dynamics are sheet-like. This is the result of the geometry-specific non-trivial formation of a peaked shock wave with a width on the order of $0.1R_0$ traversing the droplet. This observation suggests that to prevent the formation of a leading peaked shock wave and spall, or a trailing rarefaction wave and a central cavity, not the pulse duration itself, the rise and fall times of the laser pulse need to be similar to τ_a. Evidently, for Gaussian pulses, this is by definition the case.

From this research, a comprehensive picture of the overall effect of pulse duration and shape on laser-induced droplet deformation is retrieved. This work may, therefore, contribute to a better understanding of laser-driven target shaping, which is an important aspect of efficient tin-droplet-based laser-produced plasma light sources for current-generation EUV lithography. In such plasma light sources, the obtainable CE is intertwined in a complex way with the characteristics of the main drive laser pulse and the distribution of the tin mass resulting from pre-pulses. Improved CE values have been claimed[43] when using finely dispersed, "volumetric" targets resulting from short-pulse interaction.[27] Advanced target shaping using sheet-type targets have demonstrated further improved CE.[44] Our work broadens the knowledge of obtainable target shapes that may be used in the industry to further improve CE. Besides CE, mitigation of debris, such as resulting from fast spallation, as covered in our work, is of importance. Lastly, optimizing the overall energy efficiency of the various pre-pulse schemes would benefit from the obtained scaling relations.

ACKNOWLEDGMENTS

This work has been carried out at the Advanced Research Center for Nanolithography (ARCNL), a public–private partnership between the University of Amsterdam (UvA), the Vrije Universiteit Amsterdam (VU), the Netherlands Organisation for Scientific Research (NWO), and the semiconductor equipment manufacturer ASML.

AUTHOR DECLARATIONS

Conflict of Interest

The authors declare no conflict of interest.

DATA AVAILABILITY

The data that support the findings of this study are available from the corresponding author upon reasonable request.

REFERENCES

[1]T. De Rességuier, L. Signor, A. Dragon, P. Severin, and M. Boustie, "Spallation in laser shock-loaded tin below and just above melting on release," J. Appl. Phys. **102**, 073535 (2007).
[2]S. A. Abrosimov, A. P. Bazhulin, V. V. Voronov, A. A. Geras'kin, I. K. Krasyuk, P. P. Pashinin, A. Y. Semenov, I. A. Stuchebryukhov, K. V. Khishchenko, and V. E. Fortov, "Specific features of the behaviour of targets under negative pressures created by a picosecond laser pulse," Quantum Electron. **43**, 246–251 (2013).
[3]I. K. Krasyuk, P. P. Pashinin, A. Y. Semenov, K. V. Khishchenko, and V. E. Fortov, "Study of extreme states of matter at high energy densities and high strain rates with powerful lasers," Laser Phys. **26**, 094001 (2016).
[4]C. A. Stan, P. R. Willmott, H. A. Stone, J. E. Koglin, M. Liang, A. L. Aquila, J. S. Robinson, K. L. Gumerlock, G. Blaj, R. G. Sierra, S. Boutet, S. A. Guillet, R. H. Curtis, S. L. Vetter, H. Loos, J. L. Turner, and F. J. Decker, "Negative pressures and spallation in water drops subjected to nanosecond shock waves," J. Phys. Chem. Lett. **7**, 2055–2062 (2016).
[5]H. Gelderblom, H. Lhuissier, A. L. Klein, W. Bouwhuis, D. Lohse, E. Villermaux, and J. H. Snoeijer, "Drop deformation by laser-pulse impact," J. Fluid Mech. **794**, 676–699 (2016).
[6]D. Kurilovich, A. L. Klein, F. Torretti, A. Lassise, R. Hoekstra, W. Ubachs, H. Gelderblom, and O. O. Versolato, "Plasma propulsion of a metallic microdroplet and its deformation upon laser impact," Phys. Rev. Appl. **6**, 014018 (2016).
[7]M. S. Krivokorytov, A. Yu Vinokhodov, Y. V. Sidelnikov, V. M. Krivtsun, V. O. Kompanets, A. A. Lash, K. N. Koshelev, V. V. Medvedev, and A. Y. Vinokhodov, "Cavitation and spallation in liquid metal droplets produced by subpicosecond pulsed laser radiation," Phys. Rev. E **95**, 031101 (2017).
[8]M. M. Basko, M. S. Krivokorytov, A. Yu. Vinokhodov, Y. V. Sidelnikov, V. M. Krivtsun, V. V. Medvedev, D. A. Kim, V. O. Kompanets, A. A. Lash, K. N. Koshelev, and A. Y. Vinokhodov, "Fragmentation dynamics of liquid-metal droplets under ultra-short laser pulses," Laser Phys. Lett. **14**, 036001 (2017).
[9]D. Kurilovich, T. D. F. Pinto, F. Torretti, R. Schupp, J. Scheers, A. S. Stodolna, H. Gelderblom, K. S. E. Eikema, S. Witte, W. Ubachs, R. Hoekstra, and O. O. Versolato, "Expansion dynamics after laser-induced cavitation in liquid tin microdroplets," Phys. Rev. Appl. **10**, 054005 (2018).
[10]M. S. Krivokorytov, Q. Zeng, B. V. Lakatosh, A. Y. Vinokhodov, Y. V. Sidelnikov, V. O. Kompanets, V. M. Krivtsun, K. N. Koshelev, C. D. Ohl, and V. V. Medvedev, "Shaping and controlled fragmentation of liquid metal droplets through cavitation," Sci. Rep. **8**, 1275 (2018).
[11]S. Y. Grigoryev, B. V. Lakatosh, M. S. Krivokorytov, V. V. Zhakhovsky, S. A. Dyachkov, D. K. Ilnitsky, K. P. Migdal, N. A. Inogamov, A. Y. Vinokhodov, V. O. Kompanets, Y. V. Sidelnikov, V. M. Krivtsun, K. N. Koshelev, and V. V. Medvedev, "Expansion and fragmentation of liquid metal droplet by a short laser pulse," Phys. Rev. Appl. **10**, 064009 (2018).
[12]O. O. Versolato, "Physics of laser-driven tin plasma sources of EUV radiation for nanolithography," Plasma Sources Sci. Technol. **28**, 083001 (2019).
[13]A. S. Stodolna, T. D. F. Pinto, F. Ali, A. Bayerle, D. Kurilovich, J. Mathijssen, R. Hoekstra, O. O. Versolato, K. S. E. Eikema, and S. Witte, "Controlling ion kinetic energy distributions in laser produced plasma sources by means of a picosecond pulse pair," J. Appl. Phys. **124**, 053303 (2018).

[14]A. L. Klein, D. Kurilovich, H. Lhuissier, O. O. Versolato, D. Lohse, E. Villermaux, and H. Gelderblom, "Drop fragmentation by laser-pulse impact," J. Fluid Mech. **893**, A7 (2020).
[15]T. D. F. Pinto, J. Mathijssen, R. Meijer, H. Zhang, A. Bayerle, D. Kurilovich, O. O. Versolato, K. S. E. Eikema, and S. Witte, "Cylindrically and non-cylindrically symmetric expansion dynamics of tin microdroplets after ultrashort laser pulse impact," Appl. Phys. A **127**, 93 (2021).
[16]R. A. Meijer, R. Schupp, J. Sheil, M. M. Basko, K. S. Eikema, O. O. Versolato, and S. Witte, "Spall-velocity reduction in double-pulse impact on tin microdroplets," Phys. Rev. Appl. **16**, 024026 (2021).
[17]I. V. Fomenkov, A. A. Schafgans, and D. C. Brandt, "Laser-produced plasma sources for high-volume-manufacturing EUV lithography," Synchrotron Radiat. News **32**, 3–8 (2019).
[18]D. Nakamura, K. Tamaru, Y. Hashimoto, T. Okada, H. Tanaka, and A. Takahashi, "Mitigation of fast ions generated from laser-produced Sn plasma for extreme ultraviolet light source by H_2 gas," J. Appl. Phys. **102**, 123310 (2007).
[19]S. S. Harilal, B. O'Shay, Y. Tao, and M. S. Tillack, "Ion debris mitigation from tin plasma using ambient gas, magnetic field and combined effects," Appl. Phys. B: Lasers Opt. **86**, 547–553 (2007).
[20]A. Bayerle, M. J. Deuzeman, S. van der Heijden, D. Kurilovich, T. D. F. Pinto, A. S. Stodolna, S. Witte, K. S. E. Eikema, W. Ubachs, R. Hoekstra, and O. O. Versolato, "Sn ion energy distributions of ns- and ps-laser produced plasmas," Plasma Sources Sci. Technol. **27**, 045001 (2018).
[21]S. A. Reijers, J. H. Snoeijer, and H. Gelderblom, "Droplet deformation by short laser-induced pressure pulses," J. Fluid Mech. **828**, 374–394 (2017).
[22]D. Hudgins and R. S. Abhari, "Rupture time of droplets impacted by a burst of picosecond laser pulses," Phys. Rev. E **99**, 031102 (2019).
[23]A. L. Klein, W. Bouwhuis, C. W. Visser, H. Lhuissier, C. Sun, J. H. Snoeijer, E. Villermaux, D. Lohse, and H. Gelderblom, "Drop shaping by laser-pulse impact," Phys. Rev. Appl. **3**, 044018 (2015).
[24]D. Kurilovich, M. M. Basko, D. A. Kim, F. Torretti, R. Schupp, J. C. Visschers, J. Scheers, R. Hoekstra, W. Ubachs, and O. O. Versolato, "Power-law scaling of plasma pressure on laser-ablated tin microdroplets," Phys. Plasmas **25**, 012709 (2018).
[25]B. Liu, D. Kurilovich, H. Gelderblom, and O. O. Versolato, "Mass loss from a stretching semitransparent sheet of liquid tin," Phys. Rev. Appl. **13**, 024035 (2020).
[26]R. A. Meijer, A. S. Stodolna, K. S. E. Eikema, and S. Witte, "High-energy Nd:YAG laser system with arbitrary sub-nanosecond pulse shaping capability," Opt. Lett. **42**, 2758–2761 (2017).
[27]D. Kurilovich, "Laser-induced dynamics of liquid tin microdroplets," Ph.D. thesis (Vrije Universiteit Amsterdam, 2019).
[28]D. Hudgins, "Advanced irradiation schemes for target shaping in droplet-based laser-produced plasma light sources," Ph.D. thesis (ETH Zürich, 2019).
[29]W. Lauterborn and C. D. Ohl, "Cavitation bubble dynamics," Ultrason. Sonochem. **4**, 65–75 (1997).
[30]C. D. Ohl and R. Ikink, "Shock-wave-induced jetting of micron-size bubbles," Phys. Rev. Lett. **90**, 214502 (2003).
[31]G. N. Sankin, W. N. Simmons, S. L. Zhu, and P. Zhong, "Shock wave interaction with laser-generated single bubbles," Phys. Rev. Lett. **95**, 034501 (2005).
[32]D. Obreschkow, P. Kobel, N. Dorsaz, A. De Bosset, C. Nicollier, and M. Farhat, "Cavitation bubble dynamics inside liquid drops in microgravity," Phys. Rev. Lett. **97**, 094502 (2006).
[33]M. M. Basko, V. G. Novikov, and A. S. Grushin, "On the structure of quasi-stationary laser ablation fronts in strongly radiating plasmas," Phys. Plasmas **22**, 053111 (2015).
[34]R. A. Meijer, "Tailored laser-droplet interaction," Ph.D. thesis (Vrije Universiteit Amsterdam, 2021).
[35]E. Villermaux and B. Bossa, "Drop fragmentation on impact," J. Fluid Mech. **668**, 412–435 (2011).
[36]J. Hernandez-Rueda, B. Liu, D. J. Hemminga, Y. Mostafa, R. A. Meijer, D. Kurilovich, H. Gelderblom, J. Sheil, and O. O. Versolato, "Early-time hydrodynamic response of a tin droplet impacted by laser-produced plasma," Phys. Rev. Research **4**, 013142 (2022).
[37]Y. B. Zel'Dovich and Y. P. Raizer, *Physics of Shock Waves and High-Temperature Hydrodynamic Phenomena* (Courier Corporation, 2002).
[38]G. E. Duvall, "Concepts of shock wave propagation," Bull. Seismol. Soc. Am. **52**, 869–893 (1962).
[39]A. Loeb and S. Eliezer, "An analytical model for creation and decay of strong shock waves caused by a trapezoidal laser pulse," Phys. Fluids **28**, 1196 (1985).
[40]A. E. Mayer and P. N. Mayer, "Strain rate dependence of spall strength for solid and molten lead and tin," Int. J. Fract. **222**, 171–195 (2020).
[41]S. A. Reijers, D. Kurilovich, F. Torretti, H. Gelderblom, and O. O. Versolato, "Laser-to-droplet alignment sensitivity relevant for laser-produced plasma sources of extreme ultraviolet light," J. Appl. Phys. **124**, 013102 (2018).
[42]D. Hudgins, N. Gambino, B. Rollinger, and R. S. Abhari, "Neutral cluster debris dynamics in droplet-based laser-produced plasma sources," J. Phys. D: Appl. Phys. **49**, 185205 (2016).
[43]J. Fujimoto, T. Hori, T. Yamazaki, and H. Mizoguchi, "Development of laser-produced tin plasma-based EUV light source technology for HVM EUV lithography," Phys. Res. Int. **2012**, 249495.
[44]I. V. Fomenkov, D. C. Brandt, A. I. Ershov, A. A. Schafgans, Y. Tao, G. O. Vaschenko, S. I. Rokitski, M. Kats, M. Vargas, M. A. Purvis, R. J. Rafac, B. La Fontaine, S. De Dea, A. LaForge, J. Stewart, S. Chang, M. Graham, D. J. Riggs, T. Taylor, M. Abraham, and D. Brown, "Light sources for high-volume manufacturing EUV lithography: Technology, performance, and power scaling," Adv. Opt. Technol. **6**, 173–186 (2017).